Forward Learning for Gradient-based Black-box Saliency Map Generation

*Zeliang Zhang, *Mingqian Feng, Jinyang Jiang, Rongyi Zhu, Yijie Peng, Chenliang Xu

Abstract

Gradient-based saliency maps are widely used to explain deep neural network decisions. However, as models become deeper and more black-box, such as in closed-source APIs like ChatGPT, computing gradients become challenging, hindering conventional explanation methods. In this work, we introduce a novel unified framework for estimating gradients in black-box settings and generating saliency maps to interpret model decisions. We employ the likelihood ratio method to estimate output-to-input gradients and utilize them for saliency map generation. Additionally, we propose blockwise computation techniques to enhance estimation accuracy. Extensive experiments in black-box settings validate the effectiveness of our method, demonstrating accurate gradient estimation and explainability of generated saliency maps. Furthermore, we showcase the scalability of our approach by applying it to explain GPT-Vision, revealing the continued relevance of gradient-based explanation methods in the era of large, closed-source, and black-box models.

1 Introduction

Deep Neural Networks (DNNs) have achieved remarkable success across a range of applications, including autonomous driving Grigorescu et al. [2020], Mozaffari et al. [2020], Huang and Chen [2020], facial recognition Mehdipour Ghazi and Kemal Ekenel [2016], Fathallah et al. [2017], Mellouk and Handouzi [2020], and clinical diagnostics De Fauw et al. [2018], Van der Laak et al. [2021], Kermany et al. [2018]. In these safety-critical domains, it is imperative that DNNs not only deliver high task performance but also provide transparent and understandable decision-making processes Tambon et al. [2022], Borg et al. [2018]. Extensive research has been devoted to demystifying DNNs, exploring various approaches such as counterfactual explanations Mothilal et al. [2020], Slack et al. [2021], attribution and activation analysis Achtibat et al. [2023], Lin et al. [2021], and saliency maps Hu et al. [2023], Tjoa and Cuntai [2022], Lorentz et al. [2021]. Of these, saliency map methods have garnered considerable interest because of their robust theoretical foundations Khorram et al. [2021], Kapishnikov et al. [2021] and superior performance. Moreover, these methods are data-centric, offering greater adaptability to different model architectures. This flexibility is particularly promising in elucidating the decisions from black-box models, which are either proprietary and cloud-based OpenAI [2020] or computationally intensive Radford et al. [2021].

The craft of saliency maps can be broadly divided into three categories: class activation mapping Zhou et al. [2016], Chattopadhay et al. [2018], Wang et al. [2020], Omeiza et al. [2019], gradient-based Sundararajan et al. [2017], Erion et al. [2021], Lundstrom et al. [2022], Yang et al. [2023] and perturbation-based methods Petsiuk et al. [2018]. Methods based on class activation map up-sample the feature map inner models for model explanation. Gradient-based methods derive the gradients of inputs relative to the output, thereby highlighting the model's areas of interest. These two approaches are intuitive and efficient but become infeasible when the model architecture is inaccessible. In contrast, perturbation-based methods involve random modifications of the inputs to identify the most sensitive regions. Although these methods are not dependent on the model's architecture,

Preprint.

compared with the other two categories, they often encounter low computational efficiency due to the vast pixel search space required.

The question naturally arises: Is it feasible to efficiently generate a high-quality saliency map explanation without access to the model's architecture, particularly in a black-box scenario?

In black-box machine learning scenarios Bodria et al. [2023], where access to full knowledge of computation graphs for optimization is unavailable, the problem becomes a Zeroth-order Optimization (ZO) problem Chen et al. [2017]. Among various ZO strategies Chen et al. [2019], Rando et al. [2024], Kozak et al. [2023], Vemula et al. [2019], the likelihood ratio method Peng et al. [2022] stands out. It pushes the parameters out of the loss function by introducing noise, allowing for unbiased gradient estimation. This method has shown competitive performance in training diverse neural networks, comparable to that achieved with backpropagation Rumelhart et al. [1986]. Such promising results inspire us to think about the plausibility of the likelihood ratio method for gradient estimation on inputs, facilitating black-box explanations through saliency maps. Motivated by this, we propose to use the likelihood ratio method to bridge the gap between gradient-based saliency map generation and black-box scenarios, as illustrated in Fig. 1, where we skip the access of backward pass of the model to get the gradient and explain the model decision.

Applying the likelihood ratio method to develop saliency maps under black-box conditions is a non-trivial task, presenting three significant challenges. First, there is the question of how to estimate gradients on images using the likelihood ratio method. Many existing studies on zeroth-order optimization assume full knowledge of the local computational structure Peng et al. [2022], Jiang et al. [2023], a luxury not available in our context where the whole model's structure, even the first layer for processing the input, is unknown. Second, we must address how to minimize the estimation variance of gradients. The likelihood ratio method, by its nature of noise injection, tends to have a high variance in gradient estimation Peng et al. [2022], Jiang et al. [2023], a problem exacerbated by the high dimensionality of images, such as those in the $\mathbb{R}^{224\times224\times3}$ space of the ImageNet-1K dataset. Accurately estimating gradients in such high-dimensional spaces is particularly challenging. Third, there is an open problem that how to decide the target for gradient computation, especially for the hard-label decision and text-based outputs of the language model.

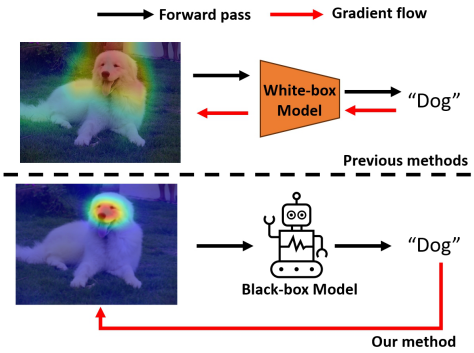

Figure 1: Previous gradient-based methods require the full knowledge of studied models for saliency map generation, which makes it impossible to be applied to explain the black-box model. Our proposed method only needs one forward pass of the studied model. It can directly get the gradient without relying on the backward pass and the knowledge of model architectures, thus enabling the black-box model decision.

In this study, we introduce a unified framework for crafting saliency maps of black models. Our approach begins with deriving estimated gradients of inputs under a black-box model set using the likelihood ratio method. Additionally, we propose a blockwise computation pattern to address the challenge of high variance in gradient estimation. We also propose two metrics to address the challenge of target selection in gradient computation, including nearest path distance and semantic distance. Finally, we conduct extensive experiments on the ImageNet-1K dataset Krizhevsky et al. [2012] to verify the effectiveness of our proposed method, including deletion&insertion game and saliency map-based adversarial attacks. To demonstrate the scalability fully, we also provide a demo application utilizing our proposed method to explain the decision of GPT-Vision.

2 Related work

2.1 Saliency maps for model explanation

Three approaches are usually employed to generate a saliency map: class activation mapping (CAM) Zhou et al. [2016], Chattopadhay et al. [2018], Wang et al. [2020], Omeiza et al. [2019], gradient-

based Sundararajan et al. [2017], Erion et al. [2021], Lundstrom et al. [2022], Yang et al. [2023], and perturbation-based methods Petsiuk et al. [2018]. CAM requires the full knowledge of model architecture and feature maps during the inference process, thus failing to work under the black-box setting.Belharbi et al. [2022], Linardatos et al. [2020], Jiang et al. [2021] Gradient-based methods Sundararajan et al. [2017, 2016] require the gradients of the decision to inputs, which treat the model as a unified module regardless of the inner structure. The perturbation-based methods Petsiuk et al. [2018], Magesh et al. [2020], Sturmfels et al. [2020] typically use randomized input sampling by applying random masks to the input image and observing the model's response to these masked inputs. With the high dimension of inputs and computation complexity of large models, it shows low efficiency and performance compared with gradient-based methods Rebuffi et al. [2020], Nauta et al. [2023].

2.2 Zeroth-order optimization

Zeroth-order optimization Wang et al. [2018], Golovin et al. [2019], Chen et al. [2019] is proposed to address challenges in optimizing the non-differential criteria. It typically uses random perturbation on input to estimate the gradient and follows the stochastic gradient descent to update the parameters of interest. Popular zeroth-order optimization methods include the simultaneous perturbation stochastic approximation (SPSA) Spall [2000, 1997], Maryak and Chin [2001], Granichin and Amelina [2014], evolutional strategy (ES) Salimans et al. [2017], and likelihood ratio (LR) Peng et al. [2022], Jiang et al. [2023]. SPSA individually perturbs each parameter and estimates the gradients. The low efficiency largely hinders its application in large-scale optimization problems. ES and LR are proposed to optimize deep learning models, which inject the noise into neuron weights and outputs respectively. Among these, LR stands out for its compelling performance in accurate gradient estimation Jiang et al. [2023]. In our work, we employ the LR to compute the gradient without reliance on the chain-rule to explain model decisions using saliency maps.

3 Methodology

In Section 3.1, we present the preliminaries of the saliency map and why the application to black-box models is limited. In Section 3.2, we introduce our framework based on likelihood ratio gradient estimation to explain black-box models. In Section 3.3, we propose the blockwise computation manner that effectively enhances the quality of the saliency map generation, especially for high-dimensional inputs and large black-box models. The pseudo-code for our framework can be found in Appendix A.

3.1 Preliminaries

Functions of gradients as saliency maps. Given any image-label pair example $(x, y) \in \mathcal{X} \times \mathcal{Y}$, with $\mathcal{X} \subset \mathbb{R}^d$ representing the domain of input images and $\mathcal{Y} = \{1, ..., C\}$ denoting the set of possible label classes, let us consider a classification neural network, $f \colon \mathcal{X} \to \mathbb{R}^C$, which assigns a predicted class activation $\hat{y}_c = f_c(x)$ for each class $c \in \mathcal{Y}$. Numerous studies Sundararajan et al. [2017], Erion et al. [2021], Lundstrom et al. [2022], Yang et al. [2023] have investigated the use of gradient-based saliency maps to visualize and elucidate the predictive mechanisms of the network f. Provided that the neural network f is differentiable almost everywhere, a gradient-based saliency map for a class c can be represented as a function dependent on the gradients of f w.r.t. inputs at dimension c, and a particular input instance x_0 as follows,

$$M_c(f, x_0) = S(g_c, x_0), \tag{1}$$

where $g_c(x_0) = \nabla_x f_c(x)|_{x=x_0}$ is the gradients of f w.r.t. inputs at x_0.

Inaccessibility of black-box models' gradients. The gradients of neural networks w.r.t. inputs are critical, as they quantify the impact of a tiny change in the input on the output and, therefore, can be linked intuitively to the importance of various input features. However, the reliance on these gradients poses a significant challenge in the context of black-box models, where the gradients are inaccessible or even the internal workings are obscured. In fact, any use of black-box modules in the model would obstruct gradient computation due to the inapplicability of the chain rule, a fundamental principle in differential calculus. This limitation severely restricts the application of gradient-based saliency map techniques in the black-box setting. Therefore, the key problem in leveraging saliency map

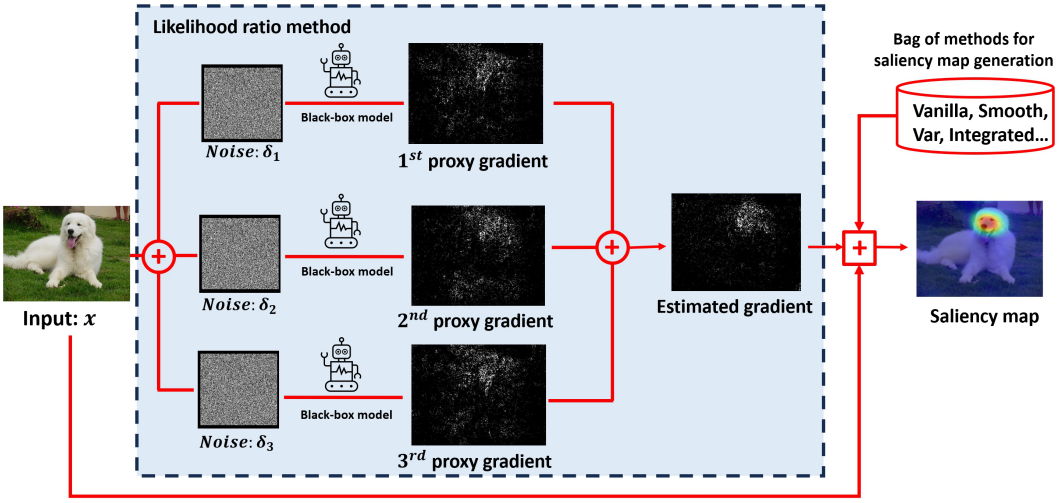

Figure 2: While the gradients of the black-box model can not be directly fetched, we use the likelihood ratio method to compute the proxy gradient of each noisy copy and obtain the estimated gradient. We incorporate the estimated gradient with gradient-based saliency map generation methods for the model explanation.

methods to interpret such models is to escape the inaccessibility of the black-box module to compute the gradients w.r.t. inputs.

3.2 Likelihood ratio method for saliency map of black-box models

In this section, we introduce a novel, unified framework for generating gradient-based saliency maps to interpret the decision of black-box models. As depicted in Fig. 2, our framework encompasses three steps. Initially, we introduce perturbations to the images by injecting the noise before the model's forward pass. Subsequently, we compute the proxy gradient of each perturbed copy respectively and then average them to approximate the true gradient. Finally, we employ the estimated gradient to craft the saliency map for the model explanation. The following paragraphs will detail the three steps in our proposed framework.

Injecting noise to inputs. Within the context of a black-box model f, which is differentiable almost everywhere but whose internal gradients are inaccessible, consider that we employ a technique of noise injection, in which we add small random noise z into the input x. Intuitively, if the noise has a neutral mean (zero) and a variance small enough, the expectation of gradient *w.r.t.* the noise-added input, $\mathbb{E}_z(g_c(x+z))$, would be close enough to the true gradient $g_c(x)$. Practically, one can easily verify that as the standard deviation σ of the noise approaches zero, the expectation of gradient w.r.t. the noise-added input converges to the true gradient, *i.e.*, $\lim_{\sigma\to 0^+}\mathbb{E}_z(g(x+z)) = g(x)$, implying the use of $\mathbb{E}_z(g_c(x+z))$ as a viable approximation of $g_c(x)$. This technique allows us to control the precision loss of expected noise-adding gradients by selecting noise z with a distribution close to 0. In many situations, such as the Gaussian noise $N(0,\sigma^2\mathbb{I})$, it is equivalent to adjusting the parameter σ.

Likelihood ratio gradient estimator. Directly computing $\mathbb{E}_z(g_c(x+z))$ still necessitates access to the gradient, which exactly contradicts our objective of addressing the black-box setting where such information is unavailable. Therefore, we propose our likelihood ratio gradient estimator for black-box models. Initially, by forwarding the noise-added input into the model, we obtain the corresponding class activation $f_c(x_0+z)$. Then, we compute the proxy gradient for each noise-added input by multiplying the class activation with the negative gradient of the noise's log probability density function. Finally, we average n samples of proxy gradients to form our likelihood ratio gradient estimator. Mathematically, this can be formalized as:

$$\hat{g}_c^{\mathrm{LR}}(x_0) \coloneqq \frac{1}{n}\sum_{i}^{n}(-f_c(x_0+z_i)\nabla_z \ln \mu_z(z_i)) \tag{2}$$

where n is the number of perturbed sample, *i.e.*, copies, $\{z_i\}_{i=1}^n$ represents the i.i.d. random noise, and $\mu_z(\cdot)$ denotes the probability density function of the injected z. Notably, when the injected

noise $z_i \overset{\text{iid}}{\sim} N(0, \sigma^2\mathbb{I})$, the likelihood ratio gradient estimator can be simplified into $\hat{g}_c^{\text{LR}}(x_0) = \frac{1}{n\sigma^2}\sum_i^n f_c(x_0 + z_i)z_i$.

Additionally, we introduce the following Theorem 1, establishing the foundation for our likelihood ratio gradient estimator for black-box models.

Theorem 1. *Assume that* $\lim_{|\zeta|\to\infty} f_c(x_0 + \zeta)\mu_z(\zeta) = 0$ *for any input* x_0. *Let* z *denote the random noise with the same distribution as* $\{z_i\}_1^n$. *Then, we have*

$$\mathbb{E}(\hat{g}_c^{LR}(x_0)) = \mathbb{E}_z(g_c(x_0 + z)). \tag{3}$$

Proof. Notice that a direct corollary from $\lim_{|\zeta|\to\infty} f_c(x_0 + \zeta)\mu_z(\zeta) = 0$ is

$$\begin{aligned} &\int_{\mathbb{R}^d} \nabla_\zeta f_c(x_0 + \zeta)\mu_z(\zeta)d\zeta + \int_{\mathbb{R}^d} f_c(x_0 + \zeta)\nabla_\zeta \mu_z(\zeta)d\zeta \\ =&\int_{\mathbb{R}^d} \nabla_\zeta \left(f_c(x_0 + \zeta)\mu_z(\zeta)\right) d\zeta = 0. \end{aligned} \tag{4}$$

Therefore, we can derive

$$\begin{aligned} \mathbb{E}_z(g_c(x_0 + z)) &= \int_{\mathbb{R}^d} \nabla_x f_c(x)|_{x=x_0+\zeta}\mu_z(\zeta)d\zeta && \triangleright \text{ by definition} \\ &= \int_{\mathbb{R}^d} \nabla_\zeta f_c(x_0 + \zeta)\mu_z(\zeta)d\zeta && \triangleright \text{ by change of variable} \\ &= -\int_{\mathbb{R}^d} f(x_0 + \zeta)\nabla_\zeta \mu_z(\zeta)d\zeta && \triangleright \text{ by Equation (4)} \\ &= \mathbb{E}_z(-f_c(x_0 + z)\nabla_z \ln \mu_z(z)) && \triangleright \text{ by derivative of } \ln \\ &= \mathbb{E}(\hat{g}_c^{\text{LR}}(x_0)). && \triangleright \text{ by i.i.d. noise} \end{aligned}$$

□

Theorem 1 indicates that the expectation of our proposed gradient estimator is the same as the expectation of gradient w.r.t. the noise-added input under a certain asymptotic growth condition, which is commonly satisfied in practice. This, together with the previous discussion about $\mathbb{E}_z(g_c(x_0 + z))$, substantiates the feasibility of utilizing $\hat{g}_c^{\text{LR}}$ as an estimator of the true gradient. While this approach introduces a certain bias, as discussed, such impacts can be effectively mitigated by carefully controlling the standard deviation of the injected noise.

Integrating with gradient-based saliency map methods. By injecting random noise into the input alongside our likelihood ratio gradient estimator, we successfully circumvent the reliance on direct access to the gradients of black-box models. This approach allows for the seamless integration of any gradient-based saliency map technique within the context of black-box models.

To illustrate, consider an arbitrary gradient-based method that generates saliency map M_c for a model f and an image x from a function S of the model's gradient w.r.t. inputs and that image, $M_c(f, x) = S(g_c, x)$, as depicted in Equation (1). For instance, in vanilla gradient Simonyan et al. [2014] we have $S(g_c, x) = g_c(x)$ while integrated gradient Sundararajan et al. [2017] defines $S(g_c, x) = (x - x') \odot \int_0^1 g_c(x' + \alpha(x - x'))d\alpha$, where x' is a predetermined baseline. Then, we substitute g_c in the function S with our likelihood ratio gradient estimator $\hat{g}_c$ defined in Equation (2), thereby enabling saliency map generation in the black-box setting, formalized as follows:

$$M_c^{LR}(f, x) = S(\hat{g}_c^{\text{LR}}, x). \tag{5}$$

3.3 Blockwise computation for scalability

Challenges with estimation variance. The aforementioned likelihood ratio method relies on the correlations between injected noise and final outputs to estimate the gradients of interested parameters or the inputs. Nevertheless, as the model becomes more complex and the input dimension d increases—a typical scenario in scaled-up models—the estimation variance, $\text{Var}([\hat{g}_c^{\text{LR}}]_i), i \in \{1, ..., d\}$, becomes unbearable. This makes it difficult to implement in real-world applications, notably including the

craft of saliency maps. Despite the requirement for only coarse gradients, high estimation variance in saliency maps associated with large images can yield vastly inconsistent attribution conclusions.

Enhancing variance reduction through blockwise estimator To make it scalable for interpreting the model decisions on high dimensional inputs, we further introduce a blockwise adaption of the likelihood ratio method for saliency map generation. Concretely, this approach involves initially selecting a rectangular segment (referred to as a "block") randomly on the original image. We adopt the sampling that ensures each pixel in the image has an equal probability q of being covered by the block. Then, we inject noise exclusively into the block area and leave the remainder of the image unchanged. Subsequently, we calculate the average of likelihood ratio proxy gradients across multiple random blocks and noise instances to form the resulting blockwise likelihood ratio gradient estimator, formalized as follows:

$$\hat{g}_c^{\text{BLR}}(x_0) \coloneqq \frac{1}{nq}\sum_{i=1}^{n}(-f_c(x_0 + J_i \odot z_i)\nabla_z \ln \mu_z(J_i \odot z_i)), \tag{6}$$

where $\{J_i\}_1^n$ represents the masks for random blocks—specifically, $[J_i]_k = 1$ if the pixel k is covered by the block and 0 otherwise. Similarly, when $\{z_i\}_1^n$ are Gaussian noise, we can simplify the blockwise likelihood ratio gradient estimator into $\hat{g}_c^{\text{BLR}}(x_0) = \frac{1}{nq\sigma^2}\sum_{i=1}^{n}(f_c(x_0 + J_i \odot z_i)J_i \odot z_i)$.

Under the same asymptotic growth condition, we derive the following Theorem 2 for the blockwise likelihood ratio gradient estimator. This theorem leads us to a direct but critical corollary, $\lim_{\sigma\to 0^+}\mathbb{E}(\hat{g}_c^{\text{BLR}}) = g_c(x)$, ensuring that blockwise estimator's efficacy in accurately estimating the gradient of black-box models with controlled standard deviation of integrated noise. The proof of the corollary is provided in detail in Appendix B.1.

Theorem 2. *Assume that* $\lim_{|\zeta|\to\infty} f_c(x_0 + \zeta)\mu_z(\zeta) = 0$ *for any input* x_0*. Then, for any noise* z *that is independent between dimensions, we have*

$$\mathbb{E}(\hat{g}_c^{BLR}(x_0)) = \mathbb{E}_{z,J}(\frac{1}{q}J \odot g_c(x_0 + J \odot z)). \tag{7}$$

Proof. Notice that when noise z is independent between dimensions, we have $\nabla_\zeta \frac{\mu_z(\zeta)}{\mu_z(J\odot\zeta)} = 0$. Then, we can obtain

$$\begin{aligned}
\mathbb{E}(\hat{g}_c^{\text{BLR}}(x_0)) &= \mathbb{E}_{z,J}(-\frac{1}{q}f_c(x_0 + J \odot z)\nabla_z \ln \mu_z(J \odot z)) \\
&= \mathbb{E}_J\left(-\frac{1}{q}\int_{\mathbb{R}^d} f_c(x_0 + J \odot \zeta)(\nabla_\zeta \mu_z(J \odot \zeta))\frac{\mu_z(\zeta)}{\mu_z(J \odot \zeta)}d\zeta\right) \\
&= \mathbb{E}_J\left(-\frac{1}{q}\int_{\mathbb{R}^d} f_c(x_0 + J \odot \zeta)\nabla_\zeta \mu_z(\zeta)d\zeta\right) \\
&= \mathbb{E}_J\left(\frac{1}{q}\int_{\mathbb{R}^d} (J \odot \nabla_x f_c(x)|_{x_0+J\odot\zeta})\mu_z(\zeta)d\zeta\right) \\
&= \mathbb{E}_{z,J}(\frac{1}{q}J \odot g_c(x_0 + J \odot z)).
\end{aligned} \tag{8}$$

□

While both the standard and blockwise likelihood ratio estimators are equivalent in terms of expected value, the implementation of blockwise computation introduces a significant advantage in variance reduction across each dimension, if the number of times that noise is added to that dimension is maintained. Formally, given the same number of copies for each input dimension in the gradient estimator computed in the standard manner in eq. (2) and the blockwise manner in eq. (6), it follows that

$$\text{Var}([\hat{g}_c^{\text{BLR}}(x_0)]_i) < \text{Var}([\hat{g}_c^{\text{LR}}(x_0)]_i),\ \forall i \in \{1, ..., d\}. \tag{9}$$

The proof and detailed analysis can be found in appendix B.2. This property supports us in reducing the gradient estimation variance for saliency map generation. We define our blockwise likelihood ratio method for saliency map generation in the same way as Equation (5) but leveraging the blockwise estimator $\hat{g}_c^{\text{BLR}}$.

3.4 The selection of the class activation

In the previous discussion, a gradient-based saliency map harnesses the gradient of the class activation w.r.t. inputs, $g_c(x_0) = \nabla_x f_c(x)|_{x=x_0}$, to explain the decision of neural networks. While we have addressed the "undifferentiable" problem due to inaccessibility for black-box models by utilizing the likelihood principle mentioned above, there remains an open question: *what if we can't access the class activation f_c of black-box models?* Here, we propose solutions for three possible scenes in real-world applications.

Soft- & Hard-label decision. When logits or confidence of models are given, we can directly use them to estimate the gradient of the loss function, *i.e.,* cross-entropy, to the inputs for saliency map generation in our framework. When only the predicted label is given, *i.e.*, the hard label, we can not directly compute the loss function for gradient estimation. To address this issue, we propose to compute the nearest path distance between the predicted class and ground truth in WorldNet as the surrogate criteria to evaluate the classification performance.

Text-based decision. Multi-modal large language models (MLLMs) output the texts for users' queries, making it difficult to define the performance criteria for gradient estimation directly. We propose two strategies to alleviate this problem:

- **Prompt construction**: When querying the decision of one image, we will additionally ask MLLMs to respond to our answer by following the format of "The input image belongs to [MASK]", where the mask is filled by taking one category of WordNet. Then, we will compute the nearest distance between two nodes, *i.e.*, one that comes from MLLMs and the ground truth, for performance evaluation and gradient estimation.

- **Semantic distance**: Besides manipulation on the text level, we propose to evaluate the performance on the latent embedding level, which better aligns with the knowledge of MLLMs. While training on similar datasets or adopting a similar backbone and pre-train/fine-tuning strategies, different models usually share similar knowledge, influencing the decision boundary. Thus, we propose to select surrogate open-source MLLMs as the criteria. Specifically, we take the text output of black-box MLLMs and the ground-truth text as the input and compute the embedding representations for the surrogate MLLMs. Then, we compute the numeric cosine similarity of these two embeddings to evaluate the performance for gradient estimation.

4 Evaluations

4.1 Experiment Setting

Models. We conduct experiments on three kinds of models, including (1) Soft-label classification models: ResNet-18 He et al. [2016], ResNet-101 He et al. [2016], ResNeXt-50 Xie et al. [2017], DenseNet-121 Huang et al. [2017], Inception-v3 Szegedy et al. [2017], and ViT-B Dosovitskiy et al. [2020]. All of these models are pre-trained on the ImageNet dataset Deng et al. [2009] ; (2) Hard-label classification model: Google's Vision API Hosseini et al. [2017]; (3) Multi-modal large language model: GPT-Vision Achiam et al. [2023].

Dataset. We randomly choose 1000 images from the ILSVRC 2012 validation set Russakovsky et al. [2015]. Each image can be classified correctly for all the models.

Implementation details. We select 5 methods as the baselines, including vanilla gradient (Vanilla) Simonyan et al. [2014], smooth grad (Smooth) Smilkov et al. [2017], variance gradient (Var) Cui et al. [2020], integrated gradient (Integ) Sundararajan et al. [2017], and random input sampling for explanation (RISE) Petsiuk et al. [2018]. Among them, only the RISE doesn't access the computational graph for gradient calculation, while others require backpropagation through models for crafting the saliency map. We integrate these gradient-based methods into our framework to match the black-box setting. Specifically, we respectively use the backpropagation and likelihood ratio to compute the gradients of outputs to the inputs and generate saliency maps based on different strategies. More detailed experiment settings can be found in Appendix C.1.

Table 1: Evaluation on the deletion (↓)&insertion (↑) task. A lower deletion score with a higher insertion score is better.

Methods	Black-box	ResNet-18		ResNeXt-50		DenseNet-121		ViT-B	
		Deletion	Insertion	Deletion	Insertion	Deletion	Insertion	Deletion	Insertion
RISE Petsiuk et al. [2018]	✓	13.3	60.3	15.8	63.1	15.7	62.9	16.5	67.3
Vanilla	×	15.7	58.2	16.9	62.5	14.8	60.5	18.3	65.2
	✓	**15.4**	**58.7**	**16.2**	**62.6**	**14.5**	**61.0**	**18.0**	**65.6**
Smooth	×	13.9	60.9	15.4	65.7	14.4	61.3	17.4	67.9
	✓	**12.4**	**61.3**	**14.8**	**66.1**	**14.0**	**62.8**	**16.6**	**68.3**
Var	×	12.1	61.3	14.7	66.4	14.4	61.9	16.9	67.4
	✓	**11.2**	**61.9**	**13.9**	**67.4**	**13.8**	**63.2**	**16.1**	**69.4**
Integ	×	11.9	62.2	13.1	68.5	13.6	65.2	15.1	70.0
	✓	**10.3**	**64.8**	**12.5**	**69.5**	**11.9**	**66.5**	**14.3**	**72.5**

4.2 Deletion&Insertion

The first evaluation task is the game of deletion&insertion Petsiuk et al. [2018]. For each image, we first use different methods to generate the saliency map, which indicates the importance of each pixel. Then, we delete or insert pixels from the original image or blank image, where the order is decided by the descending importance. The deletion&insertion scores are the changes in output probability. A lower deletion score with a higher insertion score indicates a better saliency map generation method. For comparison, we first use baseline methods to generate saliency maps of each image for four models, including ResNet-18, ResNeXt-50, DenseNet-121, and ViT-B, under the white-box setting, *i.e.*, the gradients can be accessed via BP. Then, we integrate them into our proposed framework to generate the estimated saliency map for model explanation under the black-box setting, *i.e.*, the gradients can be only estimated by LR.

We present the results in the Tab. 1. We can notice that, compared to most gradient-based methods, RISE is limited by the problem of sampling efficiency and has a marginal performance degradation of 0.85% on average. It suggests that the gradient is a comparably more significant and direct signal to explain the model's decision. Among the gradient-based methods, the integration gradient method for saliency map generation is the best under the white-box setting. Moving to the black-box setting where the gradient can not be accessible by the backpropagation, we can see that the use of the LR technique for gradient estimation not only makes these methods still work but also further boosts the performance with an average improvement of 0.92%. Especially the integration of integrated gradients into our framework achieves a further improvement of 1.51% under the black-box setting compared with the integrated gradient under the white-box setting. The introduction of noise in gradient estimation works as a smooth technique to sufficiently alleviate the overfitting problem of gradients and enhance the generalization for capturing more robust features.

4.3 Black-box Adversarial Attacks

We then evaluate the quality of the generated saliency maps on the task of black-box adversarial attacks, including surrogate model-based transferable adversarial attacks Wang et al. [2023a,b], Zhang et al. [2024] and hard-label decision-based attacks Cheng et al. [2019], Li et al. [2020], Wang et al. [2022].

Transferable Adversarial Attack. Recent studies have identified that the adversarial examples generated by attacking surrogate models on the saliency maps are more transferable to fool black-box models Wu et al. [2020], Ma et al. [2023]. Intuitively, this is probably because the saliency maps capture more robust features shared between different models. The better the saliency maps explain the models well, the higher the attack success rates of adversarial examples against the victim models. In our evaluation, we respectively use the ResNet-101 and Inception-v3 as surrogate models to generate the saliency map and attack other models, including the ResNet-18, ResNeXt-50, DenseNet-121, and ViT-B. We integrate the different saliency map generation methods into the framework of MIG Ma et al. [2023]. For reference, when generating the saliency maps, we respectively use the white-box and black-box settings. We set the number of iterations for the attack as 10, the maximum perturbation budget as $10/255$, and the momentum decay factor as 1.0.

The results are shown in Tab. 2. We can see that a better quality saliency map boosts the adversarial transferability, where there is a clear attack success rate improvement of 8.3% on average from the vanilla gradient to integrated gradients. Besides, compared with using the gradients derived from

Table 2: Attach success rate (%) of transferable adversarial attacks. A higher attack success rate indicates a better method.

Methods	Black-box	Resnet-18	ResNet-101	ResNeXt-50	DenseNet-121	Inception-v3	ViT-B
RISE Petsiuk et al. [2018]	✓	21.5	23.6	22.7	25.1	19.9	34.9
Vanilla	×	58.3	69.3	66.1	37.6	42.5	81.0
	✓	**59.6**	**70.1**	**66.9**	**38.4**	**43.7**	**81.6**
Smooth	×	60.3	69.5	68.2	38.5	44.6	80.3
	✓	**62.4**	**71.9**	**69.8**	**38.6**	**45.7**	**82.0**
Var	×	60.5	70.2	69.7	38.9	45.2	81.9
	✓	**62.4**	**73.8**	**70.5**	**39.4**	**46.2**	**82.3**
Integ	×	69.1	75.6	77.3	45.2	52.5	84.9
	✓	**72.3**	**78.5**	**78.1**	**46.2**	**53.2**	**86.7**

Table 3: The number of images successfully fooling the Google's Vision API under different root mean square error $(0.1/0.05/0/01)$. We use different methods to attack Google's Vision API directly with the maximum number of queries of $10,000$.

Method	OPT	SignOPT	HSJA	QEBA	GeoDA	Surfree	TA	**Ours**
ASR	9/4/4	13/6/5	17/8/8	15/9/6	21/15/11	23/10/9	32/17/14	**41/33/25**

the backpropagation, the gradient estimated by our proposed framework shows good generalization between models, indicating a better capacity to capture more general and robust features. By integrating different saliency map generation methods into our proposed framework under the black-box setting, the adversarial attack success rates are improved with 1.4% on average. Specifically, the integrated gradients with our framework under the black-box setting achieve the best performance with a clear margin of 1.7% against the runner-up method.

Hard-Label Decision-based Attack. Compared with surrogate model-based transferable adversarial attacks, the hard-label decision-based attack generally fools the victim model by only accessing the API without relying on using surrogate models to craft adversarial perturbation. Attackers can only access the hard-label decision without the model confidence, hindering the direct computation of the loss function. Rather than conventional methods that query the model multiple times iteratively to update adversarial perturbation, we can employ our proposed framework to attack images by continuously perturbing the area of model interests. We integrate our framework into MI-FGSM Dong et al. [2018] and compare the performance with advanced hard-label decision-based attacks, including SignOPT Cheng et al. [2020], HSJA Chen et al. [2020], QEBA Li et al. [2020], GeoDA Rahmati et al. [2020], and TA Wang et al. [2022]. To save the query budget, we adopt the vanilla gradient as the base strategy to generate the saliency map, where the gradient is computed by the likelihood ratio method. We randomly select 50 images from our test set and use different methods to generate adversarial examples to attack Google's Vision API. The number of queries is limited to $10,000$. We respectively evaluate the attack success rate (ASR) under different magnitudes of perturbation, which is computed by the root mean squared error, including 0.1, 0.05, and 0.01.

The results are shown in Tab. 3. We can see that our method achieves a marginal performance improvement of 28.1% on average against the runner-up method TA. This result sufficiently shows

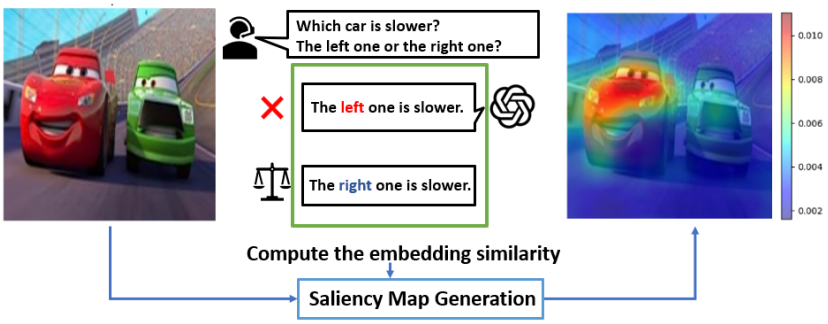

Figure 3: Explaining the GPT-Vision in the visual-question answering task.

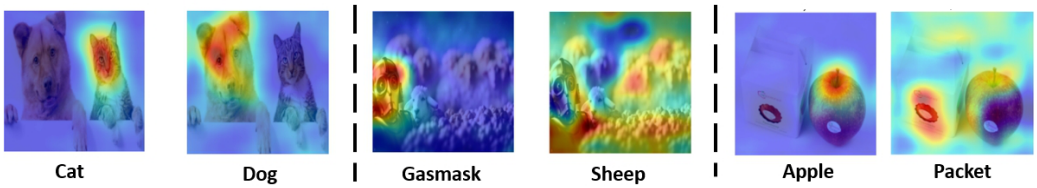

Figure 4: Explain the decision of GPT-Vision using our proposed framework.

the crucial role of gradients in the optimization process, which poses the most straightforward and efficient direction toward optima. Compared with others' heuristic methods by continuous query, our method achieves the best black-box attack performance by estimating the unbiased gradient with low variance.

4.4 Demo Application for Explaining GPT-Vision

To further demonstrate the scalability of our framework, we present a demo application to explain the decision of GPT-Vision, whose output is text. For a simple classification task, we use the prompt construction strategy as introduced in Sec. 3.4 as the criteria to estimate the gradient and generate the saliency map. For complex visual question-answering tasks, as shown in Fig. 3, we use the semantic distance in embedding space as the criteria to estimate the gradient and compute the saliency map for model explanation.

For the case in Fig. 3, we can see the GPT-V gives a wrong answer (the left one), while the right one is slower in fact. It is also a well-known hallucination of LLM. When we use our proposed framework to estimate the gradient and generate the saliency map, it is clear that GPT-V puts the most attention on the left car while nearly leaving no attention on the right. The alignment of the model decision and corresponding saliency map indicate that GPT-V can not understand the concept of speed from the image well, making itself confused when making the decision.

As shown in Fig. 4, we also present several examples of using saliency maps to explain the GPT-Vision's decision in the simple classification task. We use the prompt construction strategy as the criteria to estimate the gradient. Each selected image contains at least two objects. For the ground-truth prompt, "The input image belongs to [MASK]", we respectively set the [MASK] as each of two objects. The results show that the saliency map can explain the decision, especially the difference between a cat and a dog. However, in complex scenes, such as lots of sheep, the saliency map can not accurately capture all targets. The interpretation of the model's decision on the "apple" also only focuses on the local part. It indicates that GPT-V relies on discriminative local features for recognition, failing to take the global structure into account. We provide more explanation results in Appendix C.2.

4.5 Ablation Study

The crucial component in our framework is the gradient estimation, which is directly employed to craft the saliency map. For a comprehensive study of our framework, we provide an ablation study on the involved gradient estimation part. We use the cosine similarity between the estimated gradient and the gradient computed by backpropagation to evaluate the accuracy of gradient estimation, indicating each component's performance in our framework.

The gradient estimation accuracy using likelihood ratio method. We vary the number of copies for images to study the performance. As shown in Tab. 4, we can see that the direct use of the likelihood ratio method on gradient computation of loss to inputs doesn't get good performance. Even with a large number of copies $10,000$, the cosine similarity between the backpropagation gradient and likelihood ratio estimated gradient is only 11.4%. While the cosine similarity becomes larger with a larger number of

Table 4: Gradient estimation accuracy by varying the number of copies.

# copies (log)	1	2	3	4	5
Similarity (%)	2.6	3.1	7.8	11.4	20.5

copies, it still poses a great challenge to deal with the balance between the number of copies (i.e., the computation efficiency) and gradient estimation performance.

The blockwise computation for variance reduction. We report the ablation study of the use of blockwise computation in Tab. 5. We vary the size ratio between the sampled boxes and the original image from 50% to 10%. Compared with Tab. 4, we can see a maximum improvement of 10.7% on the gradient estimation accuracy in terms of the cosine similarity. With reduced box size for injecting noise and gradient estimation in each forward pass, the accuracy can be continuously improved. Specifically, it has a high gradient estimation accuracy of 38.5% when taking the 10% of the original image size as boxes. Results show that selecting smaller masks can significantly improve the gradient estimation accuracy.

Table 5: Variance reduction using the blockwise technique with different sizes.

Relative size	10%	20%	30%	40%	50%
Similarity (%)	38.5	26.3	22.1	17.5	14.8

5 Conclusion

In our work, we propose a unified framework for gradient-based saliency map generation of black-box models. We motivate the application of the likelihood ratio method in training neural networks with only one forward and design a pipeline to employ it in gradient estimation for saliency map generation, especially in black-box scenarios. To mitigate the large gradient estimation variance, we further propose the blockwise computation technique, which trades the computation cost with the task performance. Extensive numeric experiment results, including the deletion&insertion game and black-box adversarial attacks, thoroughly demonstrate the effectiveness of our proposed method in saliency map generation. We also apply our method in explaining the multi-modal large language model, *i.e.*, GPT-Vision, to further verify the scalability of our pipeline in real-world applications. This study simulates a new path to explain the black-box model for future studies.

References

Josh Achiam, Steven Adler, Sandhini Agarwal, Lama Ahmad, Ilge Akkaya, Florencia Leoni Aleman, Diogo Almeida, Janko Altenschmidt, Sam Altman, Shyamal Anadkat, et al. Gpt-4 technical report. *arXiv preprint arXiv:2303.08774*, 2023.

Reduan Achtibat, Maximilian Dreyer, Ilona Eisenbraun, Sebastian Bosse, Thomas Wiegand, Wojciech Samek, and Sebastian Lapuschkin. From attribution maps to human-understandable explanations through concept relevance propagation. *Nature Machine Intelligence*, 5(9):1006–1019, 2023.

Soufiane Belharbi, Aydin Sarraf, Marco Pedersoli, Ismail Ben Ayed, Luke McCaffrey, and Eric Granger. F-cam: Full resolution class activation maps via guided parametric upscaling. In *Proceedings of the IEEE/CVF Winter Conference on Applications of Computer Vision*, pages 3490–3499, 2022.

Francesco Bodria, Fosca Giannotti, Riccardo Guidotti, Francesca Naretto, Dino Pedreschi, and Salvatore Rinzivillo. Benchmarking and survey of explanation methods for black box models. *Data Mining and Knowledge Discovery*, pages 1–60, 2023.

Markus Borg, Cristofer Englund, Krzysztof Wnuk, Boris Duran, Christoffer Levandowski, Shenjian Gao, Yanwen Tan, Henrik Kaijser, Henrik Lönn, and Jonas Törnqvist. Safely entering the deep: A review of verification and validation for machine learning and a challenge elicitation in the automotive industry. *arXiv preprint arXiv:1812.05389*, 2018.

Aditya Chattopadhay, Anirban Sarkar, Prantik Howlader, and Vineeth N Balasubramanian. Grad-cam++: Generalized gradient-based visual explanations for deep convolutional networks. In *2018 IEEE winter conference on applications of computer vision (WACV)*, pages 839–847. IEEE, 2018.

Jianbo Chen, Michael I. Jordan, and Martin J. Wainwright. Hopskipjumpattack: A query-efficient decision-based attack. In *2020 IEEE Symposium on Security and Privacy, SP 2020, San Francisco, CA, USA, May 18-21, 2020*, pages 1277–1294. IEEE, 2020.

Pin-Yu Chen, Huan Zhang, Yash Sharma, Jinfeng Yi, and Cho-Jui Hsieh. Zoo: Zeroth order optimization based black-box attacks to deep neural networks without training substitute models. In *Proceedings of the 10th ACM workshop on artificial intelligence and security*, pages 15–26, 2017.

Xiangyi Chen, Sijia Liu, Kaidi Xu, Xingguo Li, Xue Lin, Mingyi Hong, and David Cox. Zo-adamm: Zeroth-order adaptive momentum method for black-box optimization. *Advances in neural information processing systems*, 32, 2019.

Minhao Cheng, Thong Le, Pin-Yu Chen, Huan Zhang, Jinfeng Yi, and Cho-Jui Hsieh. Query-efficient hard-label black-box attack: An optimization-based approach. In *7th International Conference on Learning Representations, ICLR 2019, New Orleans, LA, USA, May 6-9, 2019*. OpenReview.net, 2019.

Minhao Cheng, Simranjit Singh, Patrick H. Chen, Pin-Yu Chen, Sijia Liu, and Cho-Jui Hsieh. Sign-opt: A query-efficient hard-label adversarial attack. In *8th International Conference on Learning Representations, ICLR 2020, Addis Ababa, Ethiopia, April 26-30, 2020*. OpenReview.net, 2020.

Zhenyu Cui, Michael C Fu, Jian-Qiang Hu, Yanchu Liu, Yijie Peng, and Lingjiong Zhu. On the variance of single-run unbiased stochastic derivative estimators. *INFORMS Journal on Computing*, 32(2):390–407, 2020.

Jeffrey De Fauw, Joseph R Ledsam, Bernardino Romera-Paredes, Stanislav Nikolov, Nenad Tomasev, Sam Blackwell, Harry Askham, Xavier Glorot, Brendan O'Donoghue, Daniel Visentin, et al. Clinically applicable deep learning for diagnosis and referral in retinal disease. *Nature medicine*, 24(9):1342–1350, 2018.

Jia Deng, Wei Dong, Richard Socher, Li-Jia Li, Kai Li, and Li Fei-Fei. Imagenet: A large-scale hierarchical image database. In *2009 IEEE conference on computer vision and pattern recognition*, pages 248–255. Ieee, 2009.

Yinpeng Dong, Fangzhou Liao, Tianyu Pang, Hang Su, Jun Zhu, Xiaolin Hu, and Jianguo Li. Boosting adversarial attacks with momentum. In *2018 IEEE Conference on Computer Vision and Pattern Recognition, CVPR 2018, Salt Lake City, UT, USA, June 18-22, 2018*, pages 9185–9193. Computer Vision Foundation / IEEE Computer Society, 2018.

Alexey Dosovitskiy, Lucas Beyer, Alexander Kolesnikov, Dirk Weissenborn, Xiaohua Zhai, Thomas Unterthiner, Mostafa Dehghani, Matthias Minderer, Georg Heigold, Sylvain Gelly, et al. An image is worth 16x16 words: Transformers for image recognition at scale. *arXiv preprint arXiv:2010.11929*, 2020.

Gabriel Erion, Joseph D Janizek, Pascal Sturmfels, Scott M Lundberg, and Su-In Lee. Improving performance of deep learning models with axiomatic attribution priors and expected gradients. *Nature machine intelligence*, 3(7):620–631, 2021.

Abir Fathallah, Lotfi Abdi, and Ali Douik. Facial expression recognition via deep learning. In *2017 IEEE/ACS 14th International Conference on Computer Systems and Applications (AICCSA)*, pages 745–750. IEEE, 2017.

Daniel Golovin, John Karro, Greg Kochanski, Chansoo Lee, Xingyou Song, and Qiuyi Zhang. Gradientless descent: High-dimensional zeroth-order optimization. *arXiv preprint arXiv:1911.06317*, 2019.

Oleg Granichin and Natalia Amelina. Simultaneous perturbation stochastic approximation for tracking under unknown but bounded disturbances. *IEEE Transactions on Automatic Control*, 60 (6):1653–1658, 2014.

Sorin Grigorescu, Bogdan Trasnea, Tiberiu Cocias, and Gigel Macesanu. A survey of deep learning techniques for autonomous driving. *Journal of Field Robotics*, 37(3):362–386, 2020.

Kaiming He, Xiangyu Zhang, Shaoqing Ren, and Jian Sun. Deep Residual Learning for Image Recognition. In *Proceedings of the IEEE/CVF Conference on Computer Vision and Pattern Recognition*, pages 770–778, 2016.

Hossein Hosseini, Baicen Xiao, and Radha Poovendran. Google's cloud vision api is not robust to noise. In *2017 16th IEEE international conference on machine learning and applications (ICMLA)*, pages 101–105. IEEE, 2017.

Brian Hu, Paul Tunison, Brandon RichardWebster, and Anthony Hoogs. Xaitk-saliency: An open source explainable ai toolkit for saliency. *Proceedings of the AAAI Conference on Artificial Intelligence*, 37(13):15760–15766, Sep. 2023. doi: 10.1609/aaai.v37i13.26871. URL `https://ojs.aaai.org/index.php/AAAI/article/view/26871`.

Gao Huang, Zhuang Liu, Laurens van der Maaten, and Kilian Q. Weinberger. Densely Connected Convolutional Networks. In *Proceedings of the IEEE/CVF Conference on Computer Vision and Pattern Recognition*, pages 2261–2269, 2017.

Yu Huang and Yue Chen. Autonomous driving with deep learning: A survey of state-of-art technologies. *arXiv preprint arXiv:2006.06091*, 2020.

Jinyang Jiang, Zeliang Zhang, Chenliang Xu, Zhaofei Yu, and Yijie Peng. One forward is enough for neural network training via likelihood ratio method. In *The Twelfth International Conference on Learning Representations*, 2023.

Peng-Tao Jiang, Chang-Bin Zhang, Qibin Hou, Ming-Ming Cheng, and Yunchao Wei. Layercam: Exploring hierarchical class activation maps for localization. *IEEE Transactions on Image Processing*, 30:5875–5888, 2021.

Andrei Kapishnikov, Subhashini Venugopalan, Besim Avci, Ben Wedin, Michael Terry, and Tolga Bolukbasi. Guided integrated gradients: An adaptive path method for removing noise. In *Proceedings of the IEEE/CVF conference on computer vision and pattern recognition*, pages 5050–5058, 2021.

Daniel S Kermany, Michael Goldbaum, Wenjia Cai, Carolina CS Valentim, Huiying Liang, Sally L Baxter, Alex McKeown, Ge Yang, Xiaokang Wu, Fangbing Yan, et al. Identifying medical diagnoses and treatable diseases by image-based deep learning. *cell*, 172(5):1122–1131, 2018.

Saeed Khorram, Tyler Lawson, and Li Fuxin. igos++ integrated gradient optimized saliency by bilateral perturbations. In *Proceedings of the Conference on Health, Inference, and Learning*, pages 174–182, 2021.

David Kozak, Cesare Molinari, Lorenzo Rosasco, Luis Tenorio, and Silvia Villa. Zeroth-order optimization with orthogonal random directions. *Mathematical Programming*, 199(1):1179–1219, 2023.

Alex Krizhevsky, Ilya Sutskever, and Geoffrey E. Hinton. ImageNet Classification with Deep Convolutional Neural Networks. In *Proceedings of the Advances in Neural Information Processing Systems*, pages 1106–1114, 2012.

Huichen Li, Xiaojun Xu, Xiaolu Zhang, Shuang Yang, and Bo Li. QEBA: Query-Efficient Boundary-Based Blackbox Attack. In *Proceedings of the IEEE/CVF Conference on Computer Vision and Pattern Recognition*, pages 1218–1227, 2020.

Yi-Shan Lin, Wen-Chuan Lee, and Z Berkay Celik. What do you see? evaluation of explainable artificial intelligence (xai) interpretability through neural backdoors. In *Proceedings of the 27th ACM SIGKDD Conference on Knowledge Discovery & Data Mining*, pages 1027–1035, 2021.

Pantelis Linardatos, Vasilis Papastefanopoulos, and Sotiris Kotsiantis. Explainable ai: A review of machine learning interpretability methods. *Entropy*, 23(1):18, 2020.

Joe Lorentz, Thomas Hartmann, Assaad Moawad, Francois Fouquet, and Djamila Aouada. Explaining defect detection with saliency maps. In *International Conference on Industrial, Engineering and Other Applications of Applied Intelligent Systems*, pages 506–518. Springer, 2021.

Daniel D Lundstrom, Tianjian Huang, and Meisam Razaviyayn. A rigorous study of integrated gradients method and extensions to internal neuron attributions. In *International Conference on Machine Learning*, pages 14485–14508. PMLR, 2022.

Wenshuo Ma, Yidong Li, Xiaofeng Jia, and Wei Xu. Transferable adversarial attack for both vision transformers and convolutional networks via momentum integrated gradients. In *IEEE/CVF International Conference on Computer Vision, ICCV 2023, Paris, France, October 1-6, 2023*, pages 4607–4616. IEEE, 2023.

Pavan Rajkumar Magesh, Richard Delwin Myloth, and Rijo Jackson Tom. An explainable machine learning model for early detection of parkinson's disease using lime on datscan imagery. *Computers in Biology and Medicine*, 126:104041, 2020.

John L Maryak and Daniel C Chin. Global random optimization by simultaneous perturbation stochastic approximation. In *Proceedings of the 2001 American control conference.(Cat. No. 01CH37148)*, volume 2, pages 756–762. IEEE, 2001.

Mostafa Mehdipour Ghazi and Hazim Kemal Ekenel. A comprehensive analysis of deep learning based representation for face recognition. In *Proceedings of the IEEE conference on computer vision and pattern recognition workshops*, pages 34–41, 2016.

Wafa Mellouk and Wahida Handouzi. Facial emotion recognition using deep learning: review and insights. *Procedia Computer Science*, 175:689–694, 2020.

Ramaravind K Mothilal, Amit Sharma, and Chenhao Tan. Explaining machine learning classifiers through diverse counterfactual explanations. In *Proceedings of the 2020 conference on fairness, accountability, and transparency*, pages 607–617, 2020.

Sajjad Mozaffari, Omar Y Al-Jarrah, Mehrdad Dianati, Paul Jennings, and Alexandros Mouzakitis. Deep learning-based vehicle behavior prediction for autonomous driving applications: A review. *IEEE Transactions on Intelligent Transportation Systems*, 23(1):33–47, 2020.

Meike Nauta, Jan Trienes, Shreyasi Pathak, Elisa Nguyen, Michelle Peters, Yasmin Schmitt, Jörg Schlötterer, Maurice van Keulen, and Christin Seifert. From anecdotal evidence to quantitative evaluation methods: A systematic review on evaluating explainable ai. *ACM Computing Surveys*, 55(13s):1–42, 2023.

Daniel Omeiza, Skyler Speakman, Celia Cintas, and Komminist Weldermariam. Smooth grad-cam++: An enhanced inference level visualization technique for deep convolutional neural network models. *arXiv preprint arXiv:1908.01224*, 2019.

OpenAI. Introducing chatgpt-3: The largest openai model yet. `https://openai.com/blog/chatgpt-3/`, 2020.

Yijie Peng, Li Xiao, Bernd Heidergott, L Jeff Hong, and Henry Lam. A new likelihood ratio method for training artificial neural networks. *INFORMS Journal on Computing*, 34(1):638–655, 2022.

Vitali Petsiuk, Abir Das, and Kate Saenko. Rise: Randomized input sampling for explanation of black-box models. *arXiv preprint arXiv:1806.07421*, 2018.

Alec Radford, Jong Wook Kim, Chris Hallacy, Aditya Ramesh, Gabriel Goh, Sandhini Agarwal, Girish Sastry, Amanda Askell, Pamela Mishkin, Jack Clark, et al. Learning transferable visual models from natural language supervision. In *International conference on machine learning*, pages 8748–8763. PMLR, 2021.

Ali Rahmati, Seyed-Mohsen Moosavi-Dezfooli, Pascal Frossard, and Huaiyu Dai. Geoda: A geometric framework for black-box adversarial attacks. In *2020 IEEE/CVF Conference on Computer Vision and Pattern Recognition, CVPR 2020, Seattle, WA, USA, June 13-19, 2020*, pages 8443–8452. Computer Vision Foundation / IEEE, 2020.

Marco Rando, Cesare Molinari, Lorenzo Rosasco, and Silvia Villa. An optimal structured zeroth-order algorithm for non-smooth optimization. *Advances in Neural Information Processing Systems*, 36, 2024.

Sylvestre-Alvise Rebuffi, Ruth Fong, Xu Ji, and Andrea Vedaldi. There and back again: Revisiting backpropagation saliency methods. In *Proceedings of the IEEE/CVF Conference on Computer Vision and Pattern Recognition*, pages 8839–8848, 2020.

David E Rumelhart, Geoffrey E Hinton, and Ronald J Williams. Learning representations by back-propagating errors. *nature*, 323(6088):533–536, 1986.

Olga Russakovsky, Jia Deng, Hao Su, Jonathan Krause, Sanjeev Satheesh, Sean Ma, Zhiheng Huang, Andrej Karpathy, Aditya Khosla, Michael Bernstein, Alexander C. Berg, and Li Fei-Fei. ImageNet Large Scale Visual Recognition Challenge. *International Journal of Computer Vision (IJCV)*, 115 (3):211–252, 2015. doi: 10.1007/s11263-015-0816-y.

Tim Salimans, Jonathan Ho, Xi Chen, Szymon Sidor, and Ilya Sutskever. Evolution strategies as a scalable alternative to reinforcement learning. *arXiv preprint arXiv:1703.03864*, 2017.

Karen Simonyan, Andrea Vedaldi, and Andrew Zisserman. Deep inside convolutional networks: Visualising image classification models and saliency maps. In Yoshua Bengio and Yann LeCun, editors, *2nd International Conference on Learning Representations, ICLR 2014, Banff, AB, Canada, April 14-16, 2014, Workshop Track Proceedings*, 2014.

Dylan Slack, Anna Hilgard, Himabindu Lakkaraju, and Sameer Singh. Counterfactual explanations can be manipulated. *Advances in neural information processing systems*, 34:62–75, 2021.

Daniel Smilkov, Nikhil Thorat, Been Kim, Fernanda Viégas, and Martin Wattenberg. Smoothgrad: removing noise by adding noise. *arXiv preprint arXiv:1706.03825*, 2017.

James C Spall. A one-measurement form of simultaneous perturbation stochastic approximation. *Automatica*, 33(1):109–112, 1997.

James C Spall. Adaptive stochastic approximation by the simultaneous perturbation method. *IEEE transactions on automatic control*, 45(10):1839–1853, 2000.

Pascal Sturmfels, Scott Lundberg, and Su-In Lee. Visualizing the impact of feature attribution baselines. *Distill*, 5(1):e22, 2020.

Mukund Sundararajan, Ankur Taly, and Qiqi Yan. Gradients of counterfactuals. *arXiv preprint arXiv:1611.02639*, 2016.

Mukund Sundararajan, Ankur Taly, and Qiqi Yan. Axiomatic attribution for deep networks. In *International conference on machine learning*, pages 3319–3328. PMLR, 2017.

Christian Szegedy, Sergey Ioffe, Vincent Vanhoucke, and Alexander A. Alemi. Inception-v4, Inception-ResNet and the Impact of Residual Connections on Learning. In *Proceedings of the AAAI Conference on Artificial Intelligence*, pages 4278–4284, 2017.

Florian Tambon, Gabriel Laberge, Le An, Amin Nikanjam, Paulina Stevia Nouwou Mindom, Yann Pequignot, Foutse Khomh, Giulio Antoniol, Ettore Merlo, and François Laviolette. How to certify machine learning based safety-critical systems? a systematic literature review. *Automated Software Engineering*, 29(2):38, 2022.

Erico Tjoa and Guan Cuntai. Quantifying explainability of saliency methods in deep neural networks with a synthetic dataset. *IEEE Transactions on Artificial Intelligence*, 2022.

Jeroen Van der Laak, Geert Litjens, and Francesco Ciompi. Deep learning in histopathology: the path to the clinic. *Nature medicine*, 27(5):775–784, 2021.

Anirudh Vemula, Wen Sun, and J Bagnell. Contrasting exploration in parameter and action space: A zeroth-order optimization perspective. In *The 22nd International Conference on Artificial Intelligence and Statistics*, pages 2926–2935. PMLR, 2019.

Haofan Wang, Zifan Wang, Mengnan Du, Fan Yang, Zijian Zhang, Sirui Ding, Piotr Mardziel, and Xia Hu. Score-cam: Score-weighted visual explanations for convolutional neural networks. In *Proceedings of the IEEE/CVF conference on computer vision and pattern recognition workshops*, pages 24–25, 2020.

Xiaosen Wang, Zeliang Zhang, Kangheng Tong, Dihong Gong, Kun He, Zhifeng Li, and Wei Liu. Triangle attack: A query-efficient decision-based adversarial attack. In Shai Avidan, Gabriel J. Brostow, Moustapha Cissé, Giovanni Maria Farinella, and Tal Hassner, editors, *Computer Vision - ECCV 2022 - 17th European Conference, Tel Aviv, Israel, October 23-27, 2022, Proceedings, Part V*, volume 13665 of *Lecture Notes in Computer Science*, pages 156–174. Springer, 2022.

Xiaosen Wang, Zeliang Zhang, and Jianping Zhang. Structure invariant transformation for better adversarial transferability. In *IEEE/CVF International Conference on Computer Vision, ICCV 2023, Paris, France, October 1-6, 2023*, pages 4584–4596. IEEE, 2023a.

Yining Wang, Simon Du, Sivaraman Balakrishnan, and Aarti Singh. Stochastic zeroth-order optimization in high dimensions. In *International conference on artificial intelligence and statistics*, pages 1356–1365. PMLR, 2018.

Zhiyuan Wang, Zeliang Zhang, Siyuan Liang, and Xiaosen Wang. Diversifying the high-level features for better adversarial transferability. In *34th British Machine Vision Conference 2022, BMVC 2022, Aberdeen, UK, November 20-24, 2023*, pages 70–76. BMVA Press, 2023b.

Weibin Wu, Yuxin Su, Xixian Chen, Shenglin Zhao, Irwin King, Michael R. Lyu, and Yu-Wing Tai. Boosting the transferability of adversarial samples via attention. In *2020 IEEE/CVF Conference on Computer Vision and Pattern Recognition, CVPR 2020, Seattle, WA, USA, June 13-19, 2020*, pages 1158–1167. Computer Vision Foundation / IEEE, 2020.

Saining Xie, Ross B. Girshick, Piotr Dollár, Zhuowen Tu, and Kaiming He. Aggregated Residual Transformations for Deep Neural Networks. In *Proceedings of the IEEE/CVF Conference on Computer Vision and Pattern Recognition*, pages 5987–5995, 2017.

Peiyu Yang, Naveed Akhtar, Zeyi Wen, and Ajmal Mian. Local path integration for attribution. *Proceedings of the AAAI Conference on Artificial Intelligence*, 37(3):3173–3180, Jun. 2023. doi: 10.1609/aaai.v37i3.25422. URL `https://ojs.aaai.org/index.php/AAAI/article/view/25422`.

Zeliang Zhang, Rongyi Zhu, Wei Yao, Xiaosen Wang, and Chenliang Xu. Bag of tricks to boost adversarial transferability. *CoRR*, abs/2401.08734, 2024.

Bolei Zhou, Aditya Khosla, Agata Lapedriza, Aude Oliva, and Antonio Torralba. Learning deep features for discriminative localization. In *Proceedings of the IEEE conference on computer vision and pattern recognition*, pages 2921–2929, 2016.

A Algorithm

We present the algorithm details in algorithm 1. To explain the decision of the black-box model f on the inputs x, we first generate n copies as $\hat{x}$. Then, we sample n independent random noise from the normal distribution to perturb the copies. Next, with the target label y, we compute the loss function value for each noisy copy and get the proxy gradient. Last, we compute the average of proxy gradients, get the estimated gradient, and employ the white-box saliency map generation to craft s.

Algorithm 1: Likelihood ratio method for saliency map generation

input : Image x with label y, black model f, loss function $\mathcal{L}(\cdot,\cdot)$, number of copies n, while-box saliency map generation method $S(\cdot)$

output : The saliency map s to interpret the decision of f on x

$\hat{x} \leftarrow$ *generate* n *copies of* x;

$\delta \leftarrow$ *sample* n *i.i.d. noise from the normal distribution*;

$\hat{x} \leftarrow \hat{x} + \delta$;

`// perturb the inputs`

$\hat{l} \leftarrow \mathcal{L}(f(\hat{x}), y)$;

$\hat{g} \leftarrow \hat{l} \cdot \delta$;

`// compute the proxy gradient`

$g \leftarrow \frac{1}{n}\hat{l}_{i=1}^{n}$;

`// compute the estimated gradient`

$s \leftarrow S(g)$

B Theory analysis

B.1 Proof of the corollary

We provide the proof of the corollary we present in section 3.3. Mathematically, the corollary is formalized as

Corollary 1. *Assume the model's gradient g_c is bounded and let the clockwise likelihood ratio gradient estimator $\hat{g}_c^{BLR}$ as defined in eq.* (6)*. Then for any input x_0, we have*

$$\lim_{\sigma \to 0^+} \mathbb{E}(\hat{g}_c^{BLR}(x_0)) = g_c(x_0) \tag{10}$$

Proof. Consider arbitrary Gaussian noise r.v. sequence $\{z_i\}_1^\infty$ that satisfies $\mathbb{E}(z_i) = 0$ and $\lim_{i\to\infty} \Sigma_i = 0$.

It follows that

$$\begin{aligned}
& z_i \xrightarrow{L_2} 0 \\
\Rightarrow\ & z_i \xrightarrow{P} 0 \\
\Rightarrow\ & J \odot z_i \xrightarrow{P} 0 \\
\Rightarrow\ & x_0 + J \odot z_i \xrightarrow{P} x_0 \\
\Rightarrow\ & g_c(x_0 + J \odot z_i) \xrightarrow{P} g_c(x_0) \\
\Rightarrow\ & \frac{1}{q} J \odot g_c(x_0 + J \odot z_i) \xrightarrow{P} \frac{1}{q} J \odot g_c(x_0) \\
\Rightarrow\ & \frac{1}{q} J \odot g_c(x_0 + J \odot z_i) \xrightarrow{L_1} \frac{1}{q} J \odot g_c(x_0) \\
\Rightarrow\ & \lim_{i\to\infty} \mathbb{E}_{z_i,J}(\frac{1}{q} J \odot g_c(x_0 + J \odot z_i)) = \mathbb{E}_{z_i,J}(\frac{1}{q} J \odot g_c(x_0)) \\
\Rightarrow\ & \lim_{i\to\infty} \mathbb{E}_{z_i,J}(\frac{1}{q} J \odot g_c(x_0 + J \odot z_i)) = g_c(x_0)
\end{aligned} \tag{11}$$

Recall that by theorem 2, we have $\mathbb{E}(\hat{g}_c^{\text{BLR}}) = \mathbb{E}_{z,J}(\frac{1}{q}J \odot g_c(x_0 + J \odot z))$. This, together with the arbitrariness of $\{z_i\}_1^\infty$ as long as $\lim_{i\to\infty} \Sigma_i = 0$, indicates that

$$\lim_{\sigma \to 0^+} \mathbb{E}(\hat{g}_c^{\text{BLR}}(x_0)) = g_c(x) \tag{12}$$

□

B.2 Analysis of variance reduction from the blockwise computation

In this discussion, we consider the Gaussian noise $z \sim N(0, \sigma^2\mathbb{I})$. Other situations are similar. Then, we have simplified estimators as follows:

$$\hat{g}_c^{\text{LR}}(x_0) = \frac{1}{n^{\text{LR}}\sigma^2} \sum_i^{n^{\text{LR}}} f_c(x_0 + z_i) z_i \tag{13}$$

$$\hat{g}_c^{\text{BLR}}(x_0) = \frac{1}{n^{\text{BLR}} q \sigma^2} \sum_{i=1}^{n^{\text{BLR}}} (f_c(x_0 + J_i \odot z_i) J_i \odot z_i). \tag{14}$$

Given the same number of copies for each input dimension in the gradient estimator computed in the standard manner, *i.e.*, $n^{\text{LR}} = n^{\text{BLR}} q$, we need to prove $\text{Var}([\hat{g}_c^{\text{LR}}(x_0)]_i) < \text{Var}([\hat{g}_c^{\text{BLR}}(x_0)]_i)$, $\forall i \in \{1, ..., d\}$. To prove this, we only need to prove $\text{Var}([f_c(x_0 + z)z]_i) < \text{Var}([f_c(x_0 + J \odot z)J \odot z]_i \mid [J]_i = 1)$. Using multivariate Taylor expansion, when σ is small, we can say

$$f_c(x_0 + z) = f_c(x_0) + \nabla_x f|_{x=x_0} \cdot z. \tag{15}$$

It follows that

$$\mathbb{E}(f_c(x_0 + z)z) = 0 + \nabla_x f|_{x=x_0} \sigma^2 \mathbb{I} = \sigma^2 \nabla_x f|_{x=x_0}. \tag{16}$$

Then, we have

$$\begin{aligned}
&\text{Var}([f_c(x_0 + z)z]_i) && (17)\\
=&\mathbb{E}([f_c(x_0 + z)z]_i^2) - \sigma^4 [\nabla_x f|_{x=x_0}]_i^2 && (18)\\
=&\mathbb{E}(f_c^2(x_0 + z)[z]_i^2) - \sigma^4 [\nabla_x f|_{x=x_0}]_i^2 && (19)\\
=&\mathbb{E}((f_c(x_0) + \nabla_x f|_{x=x_0} \cdot z)^2 [z]_i^2) - \sigma^4 [\nabla_x f|_{x=x_0}]_i^2 && (20)\\
=&f_c^2(x_0)\sigma^2 + 2\sigma^4 [\nabla_x f|_{x=x_0}]_i^2 + \sigma^4 \sum_{k=1,k\neq i}^{d} [\nabla_x f|_{x=x_0}]_k^2 && (21)
\end{aligned}$$

Similarly, we have

$$\mathbb{E}(f_c(x_0 + J \odot z)J \odot z \mid [J]_i = 1) = \sigma^2 [\nabla_x f|_{x=x_0}]_i \tag{22}$$

and then

$$\begin{aligned}
&\text{Var}([f_c(x_0 + J \odot z)J \odot z]_i \mid [J]_i = 1) && (23)\\
=&\mathbb{E}([f_c(x_0 + J \odot z)J \odot z]_i^2 \mid [J]_i = 1) - \sigma^4 [\nabla_x f|_{x=x_0}]_i^2 && (24)\\
\approx&f_c^2(x_0)\sigma^2 + 2\sigma^4 [\nabla_x f|_{x=x_0}]_i^2 + q\sigma^4 \sum_{k=1,k\neq i}^{d} [\nabla_x f|_{x=x_0}]_k^2 && (25)\\
<&\text{Var}([f_c(x_0 + z)z]_i), && (26)
\end{aligned}$$

if $\exists k \in \{1, ..., d\}$, $k \neq i$, such that $[\nabla_x f|_{x=x_0}]_k \neq 0$.

C Experiment details

C.1 Hyper-parameter setting

For the Smooth- and Var-Grad, we take the variance of injected Gaussian noise as 1.0. For the integrated gradient, we take the number of steps for integration as 50. For the RISE, we take the number of samples as 8000 following the official implementation. For our method, we take the number of copies n as $1,000$, the number of blocks as 3×3, and the variance of injected Gaussian noise as 1.0. For the selected adversarial attack methods, we adopt the hyper-parameters for baselines exactly the same as in the original papers.

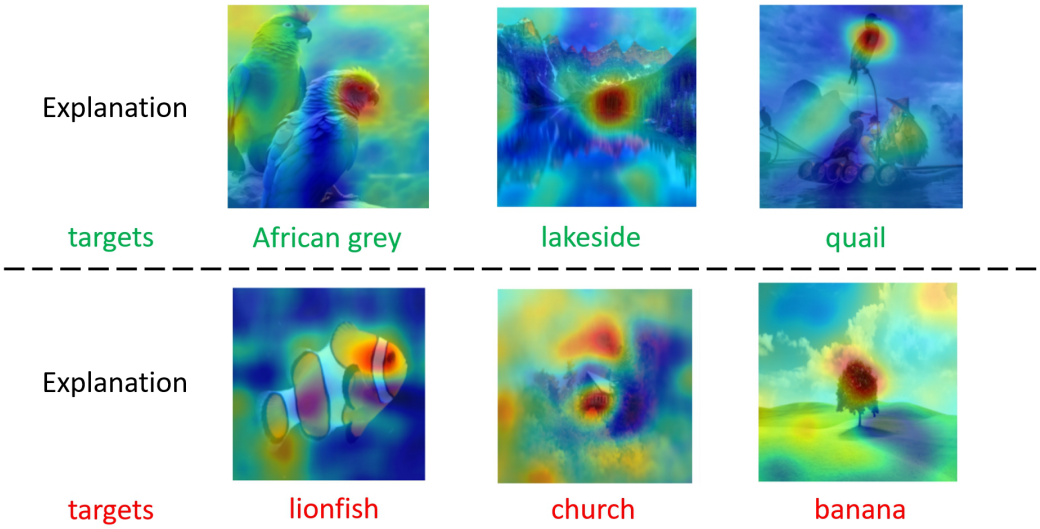

Figure C1: Explanation of GPT-Vision on two groups of data. We set the correct targets, *i.e.*, the targets to be explained is aligned with the ground-truth label of the image, for decision explanation at the first group (Line 1), while we set the wrong targets at the second group (Line 2).

C.2 More explanation results

We provide more explanation results in fig. C1. The studied black-box model is GPT-Vision. We use the hard label criteria for the gradient estimation. We select 6 images and divide them into two groups. For the first group, we want to get the explanation for why it is classified into the correct category. For the other group, we randomly select another category, and want to get the explanation about how can we classify it into this wrong category. The correct and wrong target categories are respectively drawn in green and red.

For the explanation of correct targets, we can see the interest of the models mostly focuses on the most discriminative region of images, like the heads of the African grey. However, due the similar features between different categories, especially for those sharing similar concepts, it may lead knowledge confusing by only focusing on local region. For example, while we want to explain the house by the church, we can see from the saliency map that another interested region is added on the sky to simulate the top of the church. A similar pheomie can be found in the explanation of the tree by banana, which share the sharp structure at the top of them. Thus, it is important for the model to consider the global structure comprehensively to make reliable predictions.